

## Steel fibre reinforced concrete pipes. Part 2: Numerical model to simulate the crushing test

### *Tubos de concreto reforçado com fibras de aço. Parte 2: Modelo numérico para simular o ensaio de compressão diametral*



**A. DE LA FUENTE**<sup>a</sup>  
albert.de.la.fuente@upc.edu

**A. D. DE FIGUEIREDO**<sup>b</sup>  
antonio.figueiredo@poli.usp.br

**A. AGUADO**<sup>c</sup>  
antonio.aguado@upc.edu

**C. MOLINS**<sup>d</sup>  
climent.molins@upc.edu

**P. J. CHAMA NETO**<sup>e</sup>  
pchama@sabesp.com.br

#### Abstract

This paper is part of an extensive work about the technological development, experimental analysis and numerical modeling of steel fibre reinforced concrete pipes. The first part ("Steel fibre reinforced concrete pipes. Part 1: technological analysis of the mechanical behavior") dealt with the technological development of the experimental campaign, the test procedure and the discussion of the structural behavior obtained for each of the dosages of fibre used. This second part deals with the aspects of numerical modeling. In this respect, a numerical model called MAP, which simulates the behavior of fibre reinforced concrete pipes with medium-low range diameters, is introduced. The bases of the numerical model are also mentioned. Subsequently, the experimental results are contrasted with those produced by the numerical model, obtaining excellent correlations. It was possible to conclude that the numerical model is a useful tool for the design of this type of pipes, which represents an important step forward to establish the structural fibres as reinforcement for concrete pipes. Finally, the design for the optimal amount of fibres for a pipe with a diameter of 400 mm is presented as an illustrating example with strategic interest.

**Keywords:** concrete pipes, fibres, crushing test, numerical model, optimal design

#### Resumo

Este artigo faz parte de um extenso trabalho relacionado ao desenvolvimento tecnológico experimental e modelagem numérica de tubos de concreto reforçados com fibra de aço. Na primeira parte ("Tubos de concreto reforçado com fibras de aço. Parte 1: Análise tecnológica do comportamento mecânico"), foi apresentado o estudo experimental com enfoque tecnológico, abordando o procedimento de ensaio e a discussão do comportamento estrutural obtido para cada consumo de fibra e tipo de reforço empregado. Nesta segunda parte, são abordados os aspectos de modelagem numérica. Neste sentido, se apresenta um modelo numérico para a simulação do comportamento de tubos de diâmetros inferiores a 1000 mm chamado MAP. São explicitadas as bases do modelo numérico e, posteriormente, seus resultados são confrontados com os obtidos experimentalmente, obtendo-se excelentes níveis de correlação. Se conclui que a ferramenta numérica é útil para a otimização deste tipo de tubos, o que representa um avanço importante para a implantação das fibras estruturais como refuerzo de tubos de concreto. Além disso, com o objetivo de proporcionar um exemplo de interesse estratégico, se apresenta a otimização do consumo de fibras para um tubo de 400 mm de diâmetro.

**Palavras-chave:** tubos de concreto, ensaio de compressão diametral, modelo numérico, otimização.

<sup>a</sup> Department of Construction Engineering, Barcelona Tech (UPC), albert.de.la.fuente@upc.edu, C/Jordi Girona Salgado, 1-3, 08034, Barcelona (Spain)

<sup>b</sup> Department of Civil Construction Engineering, University of São Paulo (USP), antonio.figueiredo@poli.usp.br. Caixa Postal 61548, CEP 05508-900. São Paulo (Brazil)

<sup>c</sup> Department of Construction Engineering, Barcelona Tech (UPC), antonio.aguado@upc.edu, C/Jordi Girona Salgado, 1-3, 08034, Barcelona (Spain)

<sup>d</sup> Department of Construction Engineering, Barcelona Tech (UPC), climent.molins@upc.edu, C/Jordi Girona Salgado, 1-3, 08034, Barcelona (Spain)

<sup>e</sup> Companhia de Saneamento Básico do Estado de São Paulo (SABESP), pchama@sabesp.com.br, São Paulo (Brazil).

## 1. Introduction

Unreinforced concrete pipes (UCP) and steel bar reinforced concrete pipes (SBRCP) are well-known and accepted solutions for drainage and sewage pipes (Viñolas *et al.* [1]).

On the other hand, fibre reinforced concrete pipes (FRCP) and those reinforced with steel rebars and fibres (SBFRCP) are other underdevelopment alternatives (Haktanir *et al.* [2], de la Fuente *et al.* [3 and 4], Figueiredo [5], Figueiredo *et al.* [6] and Lambrechts [7]). In this respect, the addition of fibres provides advantages from both the technical and the economic point of view. From the technical point of view, a substantial improvement of several mechanical properties of concrete is achieved (As'ad *et al.* [8]), especially with the addition of metallic fibres (Blanco [9]). Likewise, the composite solution leads to a positive structural synergy: the steel rebars perform the main strength function (Chiaia *et al.* [10]), whereas the fibres bridge the cracks, reducing their average spacing and width. The fibres also contribute to the strength function (Blanco *et al.* [11]). The use of fibres also contribute economically, because allows saving up on the assembling operations related to conventional reinforcement, reducing labor force, equipment use, and associated risks (de la Fuente *et al.* [12]).

FRCP and SBFRCP have already been considered as alternatives for UCP and SBRCP in several experimental campaigns both in Brazil (see Figueiredo *et al.* [6 and 13]) and Spain (see de la Fuente *et al.* [3]). However, their introduction in the market is under progress due to several factors such as: (1) the risk

of damage when FRCP are manipulated; (2) the lack of calculation methods for this type of material, and (3) the difficulty to overcome the inertia towards change (Parrot [14]). Nonetheless, nowadays there are solutions for such problems: (1) polishing with emery powder in order to remove imperfections and avoid possible injuries; (2) constitutive equations to consider the tensile behavior of the steel fibre reinforced concrete (SFRC) (Hillerborg *et al.* [15], Vandewalle *et al.* [16] and Laranjeira *et al.* [17]), and (3) it has been verified that the incorporation of fibres improves the response of the pipe and leads to a global reduction of costs (Pedersen 1992 [18]).

Another relevant aspect related to FRCP and SBFRCP technology is the lack of recommendations and simplified calculation methods. Because of this, the design of FRCP and SBFRCP is normally carried out by trial and error: trying out several dosages and/or concrete thickness until finding an optimal amount of fibres that meet the requirements of the desired strength class in the crushing test (CT) (Figure [1]). This design procedure is hardly operative, uneconomical and inefficient due to the variety of diameters, thickness, strength classes, types of fibres and the factory limitations. For this reason, it is necessary to develop analytical and/or numerical tools that would make possible to carry out the optimal design and the verification of concrete pipes (CP), especially FRCP and SBFRCP, in order to avoid the regular procedures traditionally used.

The aim of this paper is, firstly, to introduce a model for the non-linear analysis of CP of medium-small diameter (less than 1000 mm) called Mechanical Analysis of Pipes (MAP) which is able to simulate the CT; and, secondly, to contrast the numerical and the experimental results in order to achieve the model validation.

Initially, a summarized exposition of the normalized CT procedure is presented. Then, the bases considered in the MAP model are mentioned, and the model results are contrasted with the results presented in the first part of this work (Figueiredo *et al.* [19]). Finally, an example of the application of MAP is presented aiming at determining the optimal amount of fibres for a pipe with 400 mm of  $D_r$ .

## 2. Crushing Test

The NBR 8890:2007 [20] specifies the procedures and all the details that should be observed during the execution of the CT. Both the cross and the longitudinal sections of the test configuration are schematically shown in Figure [2].

The load process and the strength requirements are function of the type of reinforcement. In the case of steel fibre reinforced concrete pipes (SFRCP) the requirements are presented below:

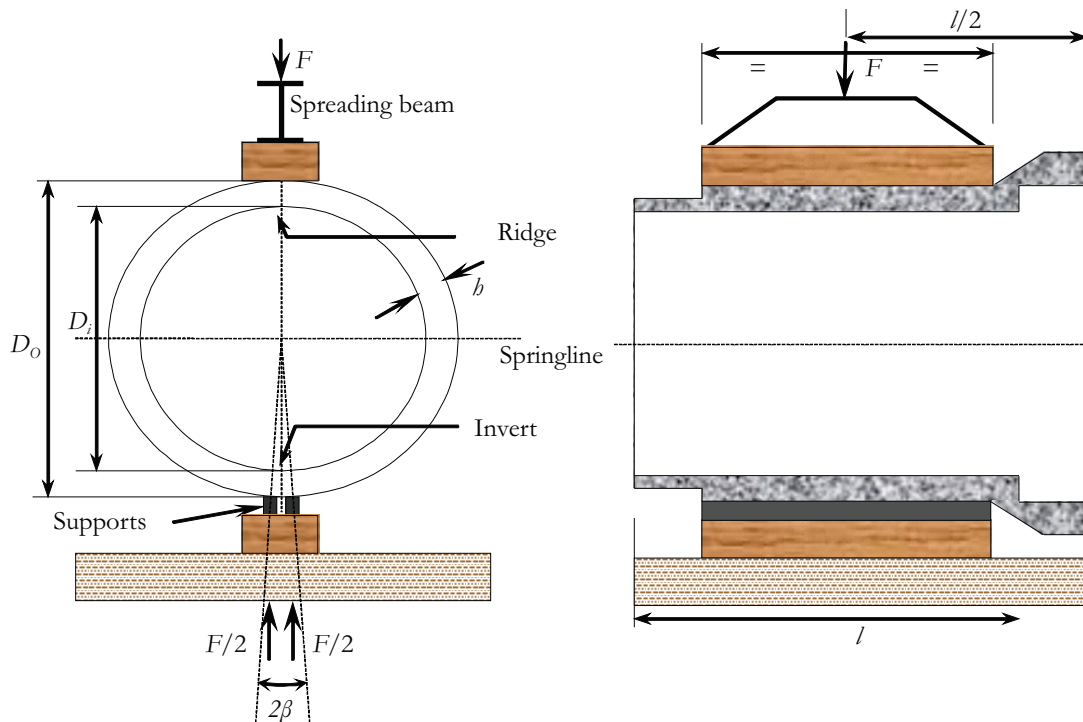
1. Withstand the proof load ( $F_p$ ) during a minute without cracking or, in other words, without exceeding the first cracking load ( $F_{cr}$ ).  $F_c$  is equivalent to the 67% of the minimum failure load ( $F_n$ ).
2. Reach the ultimate failure load  $F_u$ , which must be higher than  $F_n$ .
3. When the load has decreased a 5% of  $F_u$ , or more, the pipe is completely downloaded and reloaded until reaching  $F_c$ . This load level must be supported for more than a minute.
4. The loading process must continue until reaching a minimum post failure load ( $F_{min, pos}$ ) equivalent to, at least, 105% of  $F_c$ .

The purpose of this cyclic loading process is to verify if the type and amount of fibres are the suitable ones to guarantee the  $F_{min, pos}$  load and, indirectly, if the fibre-concrete anchorage and the post-peak strength of SFRC are appropriate (Figueiredo [5]).

Figure 1 – Three edge bearing test or crushing test



Figure 2 - Crushing test: (a) cross section and (b) longitudinal section



### 3. Model for the simulation of the crushing test

The required subroutine for the simulation of the CT up to high displacement levels should take in to account paramount aspects as the cracking the post-failure response of the materials and the modeling of the SFRC behavior. In that sense, the Analysis of Evolutive Sections (AES) introduced in de la Fuente *et al.* [21] was used in order to deal with these aspects.

On the other hand, the MAP routine, which includes the AES model, was also developed. The bases for the structural model were already suggested by Pedersen [22] for the analysis of pipes with a small diameter. However, for this work, several changes were made as regards the behavior at the sectional level, the constitutive equations of SFRC and the possibility of considering the coexistence of steel rebars and structural fibres as reinforcement.

This section puts forward the main foundations of the AES model, highlighting the modifications introduced for this work, as well as the analytical equations of the MAP model and the calculation algorithm.

#### 3.2 Sectional analysis model

##### 3.2.1 Modeling the materials

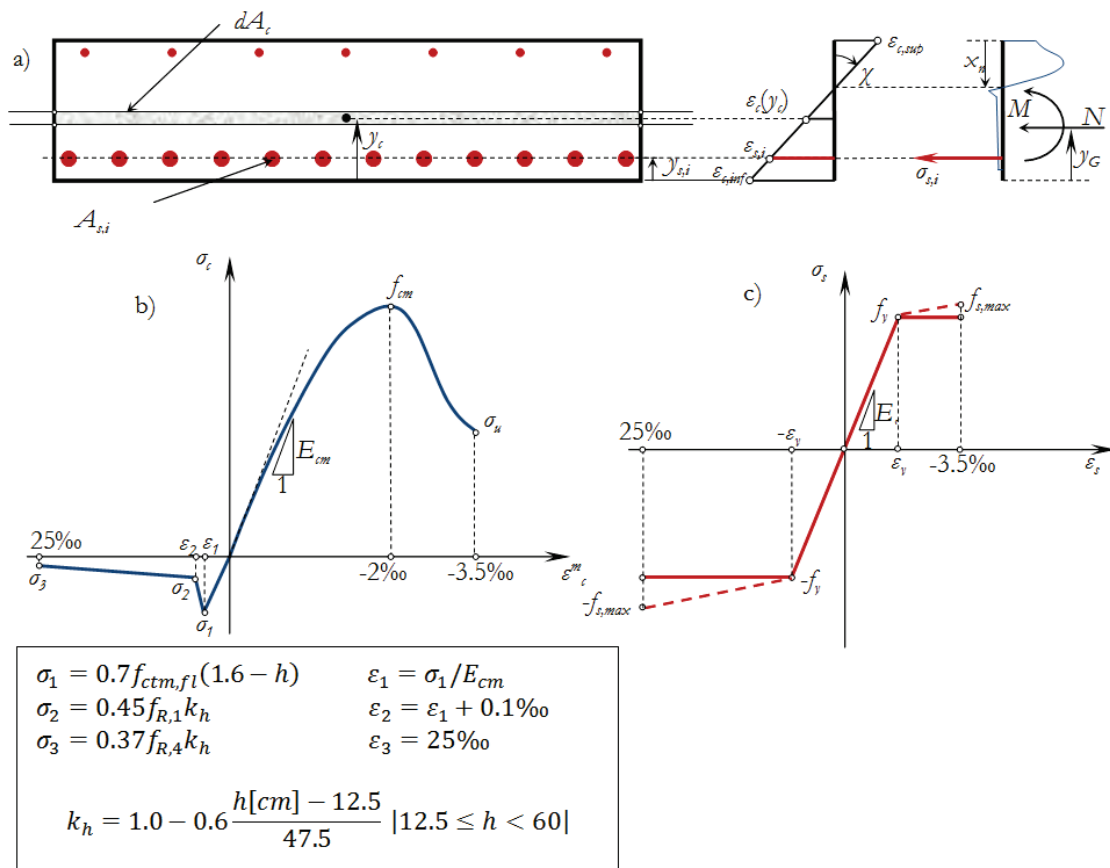
The AES model discretizes the concrete in 2-D differential elements ( $dA_c$ ), and the steel rebars in elements with concentrated area  $A_{s,i}$  in its gravity center  $y_{s,i}$ . Then, it assigns the suitable con-

stitutive model to each material and integrates the stresses resulting from a given strain plane (see Figure [3a]). The total concrete strain  $\epsilon_c(t, t_0)$ , assessed at an instant of time  $t$ , is considered to be the sum of the mechanical strains  $\epsilon_c^m(t_0)$ , produced instantaneously at  $t_0$ , and the non-mechanical strains  $\epsilon_c^{nm}(t, t_0)$  (see de la Fuente *et al.* [21] and Marí *et al.* [23]). In this paper,  $\epsilon_c^{nm}(t, t_0)$  are not considered since the test only takes a few minutes to be executed, insufficient time to present non-mechanical strains due to the concrete creep. Likewise, according to Heger [24], shrinkage hardly influences the stress state of the pipe cross section; hence, it is also disregarded in this model.

For the simulation of the concrete compressive behavior the diagram suggested by Thorenfeldt *et al.* [25] is used, since it could be adjusted correctly to a wide range of concrete strengths and suitably simulates the post-failure response. On the other hand, the tensile behavior and concrete stiffening between cracks is described by means of the equation proposed in Collins *et al.* [26].

According to Bencardino *et al.* [27], the inclusion of metallic fibres modifies the SFRC compressive behavior depending on the volume of fibres used. In this respect, the expression suggested by Barros *et al.* [28] fits properly the uniaxial compressive behavior in the post-failure regime of SFRC. On the other hand, the simulation of its tensile behavior has been dealt by means of the  $\sigma_c$ - $\epsilon_c$  model (see Figure [3b]) proposed in (Vandewalle *et al.* [16]), because it has already been used in several numerical-experimental contrasting tests (see Pujadas [29]), guaranteeing good results.

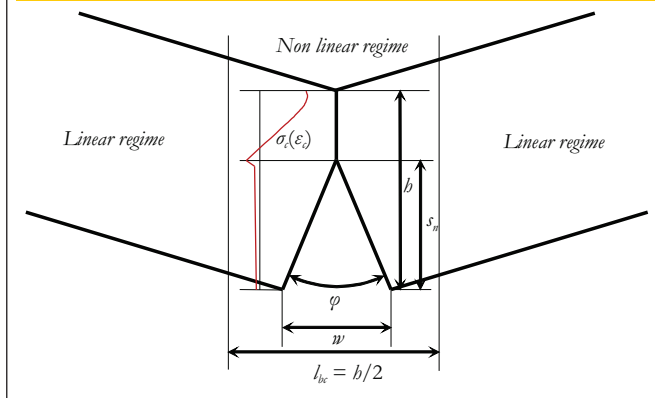
Figure 3 - (a) Cross section discretization, (b) Compression and tensile SFRC laws and (c) constitutive diagram adopted to simulate the passive steel behavior



The value of the crack width ( $w$ ) is calculated considering that the crack surfaces rotate as a rigid body (see Figure [4]), forming a  $\varphi$  angle between the crack faces (Eq. 1). This angle is related to the sectional curva-

ture  $\chi$  by means of the length of the hinge  $l_{bc}$  through Eq. 2 (see Pedersen [30]). The value of  $l_{bc}$  varies depending on the stress level of the section; however, some authors (Pedersen [30] and Olesen [31]) establish it as a constant value of  $h/2$ , and still others (Casanova [32]) propose that it should vary depending on the crack height ( $s_n$ ). For this paper, a constant value of  $h/2$  for  $l_{bc}$  has been adopted, following the recommendations proposed by Pedersen [30] for the analysis of FRCP.

Figure 4 - Rigid body schema adopted to assess  $w$



$$w = s_n \tan \varphi \tag{1}$$

$$\varphi = l_{bc} \chi \tag{2}$$

The steel rebars are modeled with a trilinear diagram, with the possibility of simulate the hardening response of the material (see Figure [3c]).

**3.2.2 Basic hypotheses about sectional behavior**

The following classical hypotheses have been adopted for the modeling the sectional behavior: (1) the sections have a symmetry axis and are subjected to straight flexo - compression; (2) perfect bond between the materials in the section; (3) sections initially planes remain planes after applying the forces; (4) shear strains are negligible and therefore are not considered; and (5) the pipe curvature does not affect on stress-strain distribution.

**3.2.3 Idealization of the section**

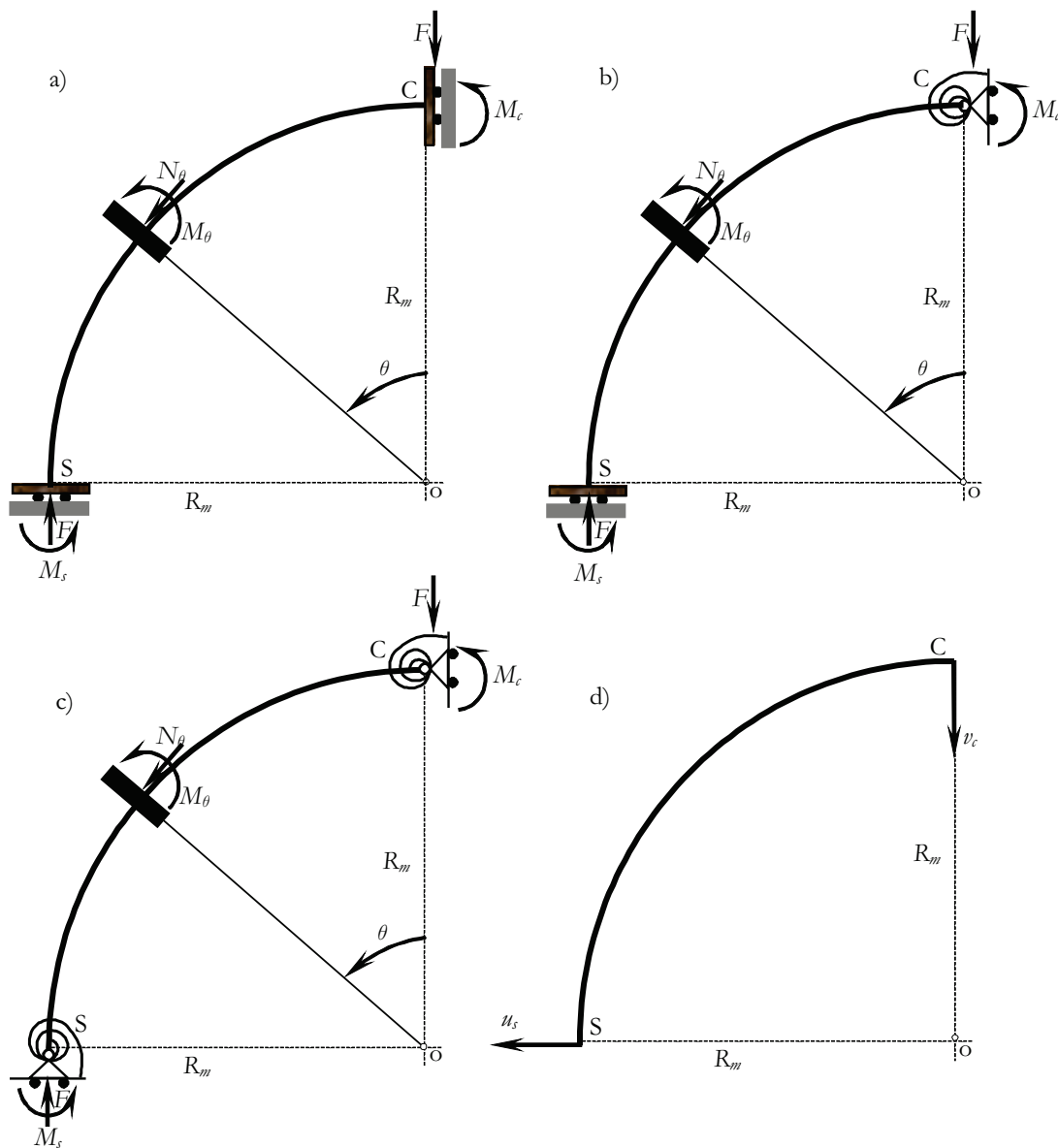
The positive signs are for: (1) the bending moments which com-

press the upper fibre; (2) the axial forces which compress the section; (3) compressive stresses and (4) the shortenings.

**3.2.4 Equilibrium and compatibility equations**

The stress-strain state (see Figure [3a]) resulting from a combination of internal efforts (normal force  $N$  and bending moment  $M$ ) is defined by the stress distribution of the materials and the plane formed by the strain in the most bottom layer of the concrete section (taken as the reference layer) and the sectional curvature ( $\epsilon_{c,inf} \chi$ ). This state is obtained by applying the internal balance equations (Eqs. 3 and 4) and establish-

Figure 5 - Schema adopted to simulate the crushing test



ing the hypothesis of perfect bond between concrete and steel (Eq. 5).

$$N = \int_{A_c} \sigma_c(\varepsilon_c) dA_c + \sum_{i=1}^{n_b} \sigma_{s,i}(\varepsilon_{s,i}) A_{s,i} \quad (3)$$

$$M + N \cdot y_G = \int_{A_c} \sigma_c(\varepsilon_c) \cdot y_c dA_c + \sum_{i=1}^{n_b} \sigma_{s,i}(\varepsilon_{s,i}) \cdot y_{s,i} A_{s,i} \quad (4)$$

$$\varepsilon(y) = \varepsilon_{c,inf} - y \cdot \chi \quad (5)$$

Eqs. 3-5 leads to a nonlinear system of equations which is solved by using the Newton-Raphson iterative method (see Yang *et al.* [33]). After solving the system, the values of the unknown parameters  $\varepsilon_{c,inf}$  and  $\chi$ , which define the strain plane, are obtained.

### 3.3 Structural analysis model

#### 3.3.1 Basic hypotheses

For the simulation of the CT (Figure [1]), the following hypotheses have been considered: (1) the structure can be idealized as a medium plane piece with a curved shape and a constant radius  $R_m$ ; (2) symmetry with regard to the vertical and the horizontal axes, so only a quarter of the pipe is simulated; (3) the initial curvature of the piece does not have an influence over the distribution of the stresses along the piece, nor over its deformed shape; (4) the axial and shear effects are disregarded in the assessment of the pipe displacements; (5) the continuous test is considered to be representative for the simulation of the FRCP behavior up to post-failure (Figueiredo [5]); and (6) three stages are considered:

- Stage 1: linear elastic stage (Figure [5a]).
- Stage 2: elastic stage with cracking at ridge (point C in Figure [5b]).
- Stage 3: elastic stage with cracking at ridge and springs (point S in Figure [5c]).

#### 3.3.2 Behavior equations

The governing equations for the structural problem implemented in MAP were deduced by Pedersen [22] for the simulation of SFRC pipes with small diameters. The strategy consists in considering that the response is represented by the three stages previously described, and that the pipe behaves elastically throughout the whole test, except the section at the ridge and at the spring line. This response pattern has also been observed in pipes tested by Figueiredo *et al.* [13]. The behavior of both sections is simulated with the AES model. This paper presents the final form of the governing equations for the problem. Their analytical deduction can be found in Pedersen [22]. They are based on the energy theorems by Castigliano (see Timoshenko [34]) and on other classical considerations about the calculation of structures.

The applied force  $F$ , and the bending moments at the ridge  $M_c$  and at the spring line  $M_s$  (see Figure [5]) are the determinant parameters. They depend on the behavior regime of the pipe and, as a consequence, the analytical formulation varies depending on the stress state of the control sections.

In the elastic regime (**Stage I**),  $M_c$  is assessed by means the linear equation (Ec. 6). Once  $M_c$  is known,  $F$  and  $M_s$  are obtained using Eq. 7 and Eq. 8, respectively. This regime ends when a crack is formed at ridge for a rotation  $\varphi_c^{crk}$  (Eq. 9).

$$M_c = E_{cm} I_{bc} \frac{\varphi_c}{l_{bc}} \quad (6)$$

$$F = \frac{\pi}{2} \frac{M_c}{R_m} \quad (7)$$

$$M_s = \left(1 - \frac{2}{\pi}\right) F R_m \quad (8)$$

$$\varphi_c^{crk} = \frac{2l_{bc} \sigma_1}{h E_{cm}} \quad (9)$$

At **Stage II**,  $M_c$  (Eq. 10) is numerically obtained with the AES model since the formation of the first crack in C leads to a non linear system (Eqs. 3-5). Then,  $F$  is calculated by means of Eq. 11 and  $M_s$  is deduced by imposing external bending moment equilibrium (Eq. 12).

$$M_c = M_c(N, \chi_c) = M_c\left(0, \frac{\varphi_c}{l_{cb}}\right) \quad (10)$$

$$F = \frac{\pi}{2R_m} M_c + \frac{E_{cm} I}{2R_m^2} (\varphi_c - \varphi_c^{crk}) \quad (11)$$

$$M_s = F R_m - M_c\left(0, \frac{\varphi_c}{l_{cb}}\right) \quad (12)$$

**Stage III** (Figure [5c]) starts when a crack is formed in the section S. This crack appears when a rotation  $\varphi_s^{crk}$  (Eq. 13) is reached. At this stage,  $F$  is calculated by means of Eq. 14,  $M_c$  (Eq. 10) is nu-

merically obtained with the AES model and  $M_s$  is deduced imposing external bending moment equilibrium (Eq. 15).

$$\varphi_s^{crk} = \frac{2I_{cb}}{hE_{cm}} \left( \frac{F}{h} + \sigma_1 \right) \quad (13)$$

$$F = \frac{\pi}{2R_m} M_c + \frac{E_{cm} I}{2R_m^2} (\varphi_c - \varphi_c^{crk} - \varphi_s + \varphi_s^{crk}) \quad (14)$$

$$M_s \left( F, \frac{\varphi_s}{I_{cb}} \right) = FR_m - M_c \left( 0, \frac{\varphi_c}{I_{cb}} \right) \quad (15)$$

The vertical displacement at the ridge ( $v_c$ ) and the horizontal displacement at the springline ( $u_s$ ) (see Figure [5d]) are calculated as a composition of the elastic strain of the pipe ( $v_c^e$  and  $u_s^e$ ) and a plastic one ( $v_c^p$  and  $u_s^p$ ) due to the rotation of the rigid body after the appearance of cracks in the critical sections.

The displacement  $v_c^e$  is calculated by means of Eq. 16 and Eq. 17.

$$v_c^e = \frac{R_m^2}{E_{cm} I} \left( M_c - \frac{1}{2} FR_m \right) \quad \text{if } \varphi_c = \varphi_c^{crk} \quad (16)$$

$$v_c^e = \frac{R_m^2}{E_{cm} I} \left( M_c - \frac{1}{2} FR_m \right) + \frac{1}{2} R_m (\varphi_c - \varphi_c^{crk}) \quad \text{if } \varphi_c > \varphi_c^{crk} \quad (17)$$

The displacement  $u_s^e$  is deduced by means of Eqs. 18 and 19.

$$u_s^e = \frac{R_m^2}{E_{cm} I} \left[ M_c \left( \frac{\pi}{2} - 1 \right) + FR_m \left( \frac{\pi}{4} - 1 \right) \right] \quad \text{if } \varphi_c \leq \varphi_c^{crk} \quad (18)$$

$$u_s^e = \frac{R_m^2}{E_{cm} I} \left[ M_c \left( \frac{\pi}{2} - 1 \right) + FR_m \left( \frac{\pi}{4} - 1 \right) \right] + \frac{1}{2} R_m (\varphi_c - \varphi_c^{crk}) \quad \text{if } \varphi_c > \varphi_c^{crk} \quad (19)$$

The displacements  $v_c^p$  and  $u_s^p$  are expressed by means of Eqs. 20-22.

$$v_c^p = u_s^p = 0 \quad \text{if } \varphi_c \leq \varphi_c^{crk} \quad (20)$$

$$v_c^p = u_s^p = \frac{1}{2} R_m (\varphi_c - \varphi_c^{crk}) \quad \text{if } \varphi_c > \varphi_c^{crk} \text{ y } \varphi_s \leq \varphi_s^{crk} \quad (21)$$

$$v_c^p = u_s^p = \frac{1}{2} R_m (\varphi_c - \varphi_c^{crk}) + \frac{1}{2} R_m (\varphi_s - \varphi_s^{crk}) \quad \text{if } \varphi_c > \varphi_c^{crk} \text{ y } \varphi_s > \varphi_s^{crk} \quad (22)$$

Relevant results are obtained with application of the MAP model, including the curves  $F-v_c$  from the CT. These curves allow understanding the behavior of the structure at each of the stages.

### 3.3.3 Solution procedure

The process is initiated with zero values for the rotations at the ridge ( $\varphi_c$ ) and spring line ( $\varphi_s$ ). The control variable is  $\varphi_c$ , which increases with variable steps depending on the behavior stage. Establishing  $N = 0$  (simple bending) for each value of  $\varphi_c$  at the ridge, the value of  $M_c$  is obtained by means of the AES model (Eq.6 for elastic regime, State I, and Eq. 10 for cracked regime, States II and III). After that, the values of  $M_s$  and  $F$  are calculated with the expressions previously presented:

- At Stage I:  $F$  is obtained with Eq. 7 and  $M_s$ , by means of Eq. 8. At this stage the whole pipe, even the critical sections, works in a linear regime.
- At Stage II:  $F$  is obtained with Eq. 11 and  $M_s$ , by means of Eq. 12. At this stage, a degree of non-linearity is introduced due to the cracking of section C ( $\varphi_c > \varphi_c^{crk}$ ), whereas section S still works in a linear regime ( $\varphi_s \leq \varphi_s^{crk}$ ). Therefore, due to the degree of hyperstatism of the system, a redistribution of moments from C to S takes place.
- At Stage III:  $F$  is obtained with Eq. 14 and  $M_s$ , by resolving Eq. 15. At this stage, unlike at the previous ones, the balance condition (Eq. 15) is non-linear due to the fact that both section C and section S have cracked. For its solution, an iterative Newton – Raphson schema was implemented (see Yang *et al.* [33]). In this sense, it has to be noticed that the section S works under a bending - compression state during the whole load process ( $N = F$  and  $M = M_s$ ).

The algorithm stops either when the maximum strain is reached at any of the two critical sections, or when the displacement  $v_c$  exceeds the fixed value pre-established by the user  $v_{c,max}$ . Once the  $F$  and  $M$  values have been obtained, the displacements in sections C and S can be assessed with Eqs. 16-22.

This procedure guarantees good results in concrete pipes with a predominantly rigid behavior: pipes with a small-medium diameter (300 - 1000 mm) and with moderate reinforcement densities. With these hypotheses, it can be guaranteed that, in most cases, the cracks are concentrated in sections C and S, while the rest of the pipe works with its entire section (de la Fuente *et al.* [3]). In the opposite case, cracks appear intermediately and the model deviates from the experimental results and it is necessary to resort to other models capable of considering the distributed cracking, such as the one presented in de la Fuente *et al.* [12].

## 4. Contrasting experimental and numerical results

With the aim of verifying the suitability of the MAP model for the simulation of the mechanical response of FRCP subjected to CT, the experimental results presented in the first part of this work (see Figueiredo *et al.* [19]) were contrasted. So, a comparison of the curves  $F-v_c$  captured during the test for the pipes with  $D_i$  of 600 mm from series 2 (displacement measured in the spigot) is done. All the pipes in these series of tests were manufactured with the same concrete composition, although there were some modifications in the water consumption in order to improve the workability due to the use of fibres (DRAMIX® RC-80/60-BN). The pipes were manufactured and tested at the same age with the aim of reaching, at least, the resistance class EA2 established in NBR 8890:2007 [20].

### 4.1 Modeling the materials

The modeling of the compressive behavior of SFRC was performed with the equation suggested by Barros *et al.* [28], considering a characteristic compressive strength ( $f_{ck}$ ) of 50 MPa at 28 days according to the tests performed during the regular quality control in the factory. On the other hand, for the simulation of its tensile response, the trilinear diagram proposed by Vandewalle *et al.* [16] was used (see Figure [3b]). However, due to the lack of flexural tests (see Vandewalle *et al.* [35]), in order to determine the values of concrete tension stress  $\sigma_p$ , the expressions (Eqs. 23-24) calibrated in Barros *et al.* [36] have been used to determine the values of the residual flexural strength  $f_{Ri}$  as a function of  $C_f$ . In this regard, the type of fibres used both in this campaign and in the one carried out by Barros *et al.* [36] are the same: (DRAMIX® RC-80/60-BN). Table [1] shows the values established for  $\sigma_p$ ,  $\epsilon_i$  and  $E_{cm}$  in order to model the tensile behavior of SFRC.

$$f_{R,1} = 0.0945C_f + 0.702 \tag{23}$$

$$f_{R,4} = 0.926 f_{R,1} \tag{24}$$

### 4.2 Results obtained

Figures 6a, 6b and 6c show the curves  $F-v_c$  obtained both experimentally (individual and average values) and numerically for pipes with  $C_f$  of 10, 20 and 40 kg/m<sup>3</sup>, respectively.

With reference to what has been previously explained in section 3 and to the requirements of the EA2 class of the NBR 8890:2007, the load  $F_{cr}$  must be equal or higher than the load  $F_c$  (90 kN), and  $F_u$  must be equal or higher than 135 kN for this type of pipes. Finally, the maximum post-failure load  $F_{max, pos}$  measured in the curve  $F-v_c$  must reach, at least, the 105% of  $F_c$  (94.5 kN). In this sense, since the test was carried out in a continuous manner, it was established that the value of  $F_{max, pos}$  is associated to a  $v_c$  of 3 mm (see Figueiredo *et al.* [19]), and is called  $F_{3mm}$ .

Based on the results presented in Fig. 6a, it is deduced that the MAP model fits properly to the experimental results for the amount of 10 kg/m<sup>3</sup>, particularly in the linear elastic regime and in the post-failure regime. For the latter, the numerical results tend toward the experimental maximum values for displacements higher than 3 mm. This might indicate that the values  $f_{R,i}$  and/or  $\sigma_i$  of the constitutive equation of tensioned SFRC (see Fig. 3b) are slightly higher than the real ones. The values for  $F_{cr}$ ,  $F_u$  and  $F_{3mm}$  obtained numerically are 98 kN, 114 kN and 88 kN, respectively. Therefore, neither  $F_u$  nor  $F_{3mm}$  reach the minimum values stipulated by NBR 8890:2007 for the EA2 class. Thus, it can be stated that, according to the model, the amount of 10 kg/m<sup>3</sup> is not enough to guarantee that level of requirements.

The results gathered in Fig. 6b, concerning the dosage of 20 kg/m<sup>3</sup>, highlight that the simulation by means of the numerical model guarantees values close to the experimental ones. Still, the model exceeds the experimental results with displacements higher than 5.5 mm, which can be due to the considered excessive values of  $f_{R,i}$  and/or  $\sigma_i$ , as in the case of pipes with 10 kg/m<sup>3</sup> of fibres for this range of displacements. The values for  $F_{cr}$ ,  $F_u$  and  $F_{3mm}$  obtained numerically are: 98 kN, 123 kN and 108 kN, respectively. Consequently, according to the model, with 20 kg/m<sup>3</sup> the EA2 class would not be reached, since the load  $F_u$  (123 kN) is lower than the required 135 kN.

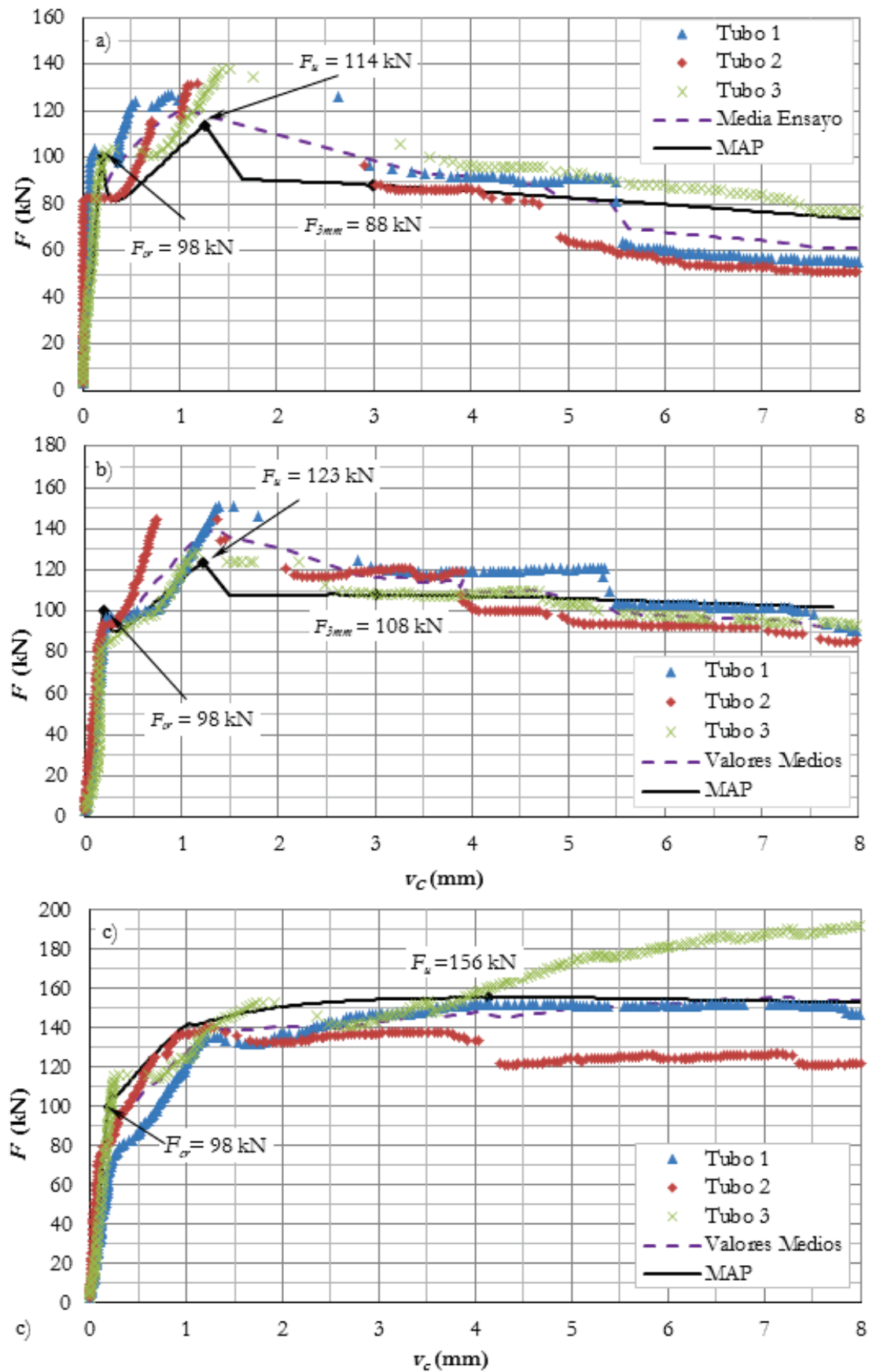
Finally, for the pipes with 40 kg/m<sup>3</sup> of fibres (Fig. 6c), it can be noticed that the numerical model adjusts suitably to the average experimental results at all the stages. In this case,  $F_{cr}$  is 98 kN and  $F_u$  is 156 kN, values higher than those specified for a pipe of 600 mm from the EA2 class (NBR 8890:2007). It should be noted that, due to the hardening behavior, there is no way to assess the

Table 1 - Parameters to simulate the tensile behavior of the SFRC for the pipe of  $D_i = 600$  mm

$C_f$ (Kg/m <sup>3</sup> )	$f_{R,1}$ (MPa)	$f_{R,4}$ (MPa)	$E_{cm}$ (MPa)	$\sigma_1^*$ (MPa)	$\epsilon_1$ (mm/m)	$\sigma_2$ (MPa)	$\epsilon_2$ (mm/m)	$\sigma_3$ (MPa)	$\epsilon_3$ (mm/m)
10	1.647	1.525	37000	4.071	0.104	0.741	0.204	0.564	25.000
20	2.592	2.400	37000	4.071	0.104	1.166	0.204	0.888	25.000
40	4.482	4.150	37000	4.071	0.104	2.017	0.204	1.536	25.000

\* This value is obtained by using the expression  $\sigma_1 = 0.30 \cdot (f_{ck})^{2/3}$  gathered in the EHE-08 (37).

Figure 6 - F- $v_c$  curves for the SFRCP with: a) 10 kg/m<sup>3</sup>, b) 20 kg/m<sup>3</sup> and c) 40 kg/m<sup>3</sup> of fibres



**Table 2 - Average experimental and numerical values of F obtained for the 2<sup>nd</sup> series of tests**

Fibre dosage (kg/m <sup>3</sup> )	Exp. (kN)	F <sub>cr</sub> MAP (kN)	ε (%)	Exp. (kN)	F <sub>u</sub> MAP (kN)	ε (%)	Exp. (kN)	F <sub>3mm</sub> MAP (kN)	ε (%)
10	94	98	-4.3	132	114	13.6	94	88	6.4
20	93	98	-5.4	142	123	13.4	116	108	6.9
40	92	98	-6.5	162	156	3.7	-	-	-

load  $F_{min,pos}$  for a displacement  $v_c$  of 3 mm as in the previous cases. However, it can be asserted that the load  $F_{min,pos}$  from these pipes exceeds the value of 94.5 kN, since the pipes with 20 kg/m<sup>3</sup> of fibres showed values 14.3% higher than this (108 kN) according to the numerical model.

Table [2] gathers the average experimental and numerical values for  $F_c$ ,  $F_u$  and  $F_{3mm}$ . The parameter  $\xi$  is the relative error of the numerical value with regard to the experimental data. Positive values of  $\xi$  indicate that the experimental data exceeds the numerical one, and vice versa. With regard to the results illustrated in Table [2], it is deduced that:

- The load  $F_{cr}$  obtained numerically is independent from the  $C_f$  since tension  $\sigma_i$  is related exclusively to the concrete matrix (see Figure [3b] and Table [1]).  $F_{cr}$  depends exclusively on  $\sigma_i$ ,  $h$  and  $D_i$  (see de la Fuente *et al.* [3]). The model tends to overestimate  $F_{cr}$  with regard to the average experimental results between a 4.3% (pipe with 10 kg/m<sup>3</sup>) and a 6.5% (pipe with 40 kg/m<sup>3</sup>). This can be due to the incorporation, during the mixing, of additional water (the bigger the amount of fibres, the bigger the quantity added) into the concrete used for the contrasted pipes (see Figueiredo *et al.* [19]).
- The model underestimates the maximum load  $F_u$  with regard to the experimental values between a 3.7% (pipe with 40 kg/m<sup>3</sup>) and a 13.6% (pipe with 10 kg/m<sup>3</sup>). For this load level, the matrix of concrete has already cracked and the fibres work with the maximum efficiency; then, the reason for this difference in the results can be due to the fact that the values of  $\sigma_i$  used in the constitutive equation might be too conservative for low levels of displacement. In this regard, de la Fuente *et al.* [38] proves that the fibres in concrete pipes manufactured with traditional systems (for example, turbo-compression) work oriented towards the stress flow, practically guaranteeing their maximum efficiency. One of the ways to consider this fact is by using an amplifi-

cation coefficient of the parameters  $\sigma_i$ . So, the use constitutive equations incorporating this effect, in order to take into account the preferential orientation of the fibres could be considered as a good alternative, as suggested by Laranjeira [39].

- As regards the load  $F_{3mm}$ , the numerical values obtained are 6.4% (10 kg/m<sup>3</sup>) and a 6.9% (20 kg/m<sup>3</sup>) lower in comparison with the experimental data. This could also be due to the underestimation of the parameters  $\sigma_i$  adopted to model the tensile response of SFRC in this regime of  $v_c$ .

To sum up, the MAP model adjusts satisfactorily to the experimental results, even considering that the input parameters of the constitutive equation used to model the tension response of SFRC are calibrated from concretes with a  $f_{ck}$  ranging between 25 and 30 MPa (see Barros *et al.* [36]), as opposed to the reported 50 MPa. Similarly, the equation used does not take into account the effect of the preferential orientation of the fibres within the wall of the pipe. Therefore, the MAP model tends to underestimate the experimental results in most of the cases, yet these differences do not exceed the 13.6%. Nevertheless, the results can be considered a success, taking into account the multitude of variables involved in the problem, their uncertainty and the difficulties for the direct experimental determination of some of them.

### 5. Example of the optimal design of the amount of fibres

The following example of MAP model application to a pipe with  $D_i$  of 400 mm,  $h$  of 67 mm and a total length of 2500 mm is purposed to illustrate the methodology of the design of the optimal  $C_f$  in SFRC. This diameter was chosen for two reasons: (1) because it is within the range of diameters for which the hypotheses from the MAP model are appropriate, and (2) because it is a commercial diameter

**Table 3 - Parameters to simulate the tensile behavior of the SFRC for the pipe of  $D_i = 400$  mm**

$C_f$ (Kg/m <sup>3</sup> )	$f_{r,1}$ (MPa)	$f_{r,4}$ (MPa)	$E_{cm}$ (MPa)	$\sigma_1$ (MPa)	$\epsilon_1$ (mm/m)	$\sigma_2$ (MPa)	$\epsilon_2$ (mm/m)	$\sigma_3$ (MPa)	$\epsilon_3$ (mm/m)
0	0.702	0.650	36000	3.795	0.105	0.316	0.205	0.241	25.000
10	1.647	1.525	36000	3.795	0.105	0.741	0.205	0.564	25.000
20	2.592	2.400	36000	3.795	0.105	1.166	0.205	0.888	25.000
30	3.537	3.275	36000	3.795	0.105	1.592	0.205	1.212	25.000

**Table 4 – Design loads for each strength class for pipes with  $D_i = 400$  mm**

	EA2	EA3	EA4
$F_c$ (kN)	60	90	120
$F_u$ (kN)	90	135	180
$F_{min,pos}$ (kN)	63	94.5	126

which lately is losing its market share in favor of the plastic pipes. Therefore, new alternatives and improvements are necessary for the concrete pipe to be competitive once again (Viñolas *et al.* [1]). For the analysis, a range of  $C_f$  between  $0 \text{ kg/m}^3$  and  $30 \text{ kg/m}^3$  was established. The first amount would correspond to an unreinforced concrete pipe (UCP), and the second one has been established as a maximum value because of economic criteria.

Likewise, the requirement of a minimum early compressive strength is necessary for demolding and to manipulate the pipe. In order to satisfy this requirement an  $f_{ck}$  of 45 MPa at age of 28 days has been assumed in order to carry out the analysis.

**Table 3** presents the values for the mechanical parameters used to simulate the tension behavior of SFRC.

The values of  $F_c$  and  $F_u$  fixed in NBR 8890:2007 for the strength classes EA2, EA3 and EA4 for pipes with  $D_i = 400$  mm are gathered in the **Table 4**.

Fig. 7 shows the curves  $F-v_c$  obtained with the MAP model. From those curves, it is deduced that:

- The load  $F_{cr}$  obtained in the four cases (96 kN) is enough to reach the load  $F_c$  stipulated in classes EA2 (60 kN) and EA3 (90 kN). However, the value of  $F_c$  for class EA4 (120 kN) cannot be reached by means of the addition of metallic fibres only (stress  $\sigma_f$  is independent from  $C_f$ ).
- The 90 kN established for  $F_u$  in class EA2 are exceeded if a fibre dosage of  $10 \text{ kg/m}^3$  (93 kN) is used. But, in order to reach the 135 kN stipulated for class EA3, according to the numerical model, at least  $30 \text{ kg/m}^3$  of fibres (136 kN) are required. On the other hand, the  $C_f$  necessary to achieve the 180 kN established for class EA4 is not under the economically competitive values.
- In order to reach the 63 kN specified for the  $F_{min,pos}$  of class EA2 and the 94.5 kN of class EA3,  $10 \text{ kg/m}^3$  (64 kN) and  $20 \text{ kg/m}^3$  (99 kN) are required, respectively.

Therefore, keeping in mind that the three strength requirements must be fulfilled simultaneously for a fixed  $C_f$ , it is possible to conclude that  $10 \text{ kg/m}^3$  of fibres would be required to achieve the EA2 class requirements, and  $30 \text{ kg/m}^3$  would be required for class EA3, according to the numerical model.

Alternatively, in order to achieve class EA4 with an economically attractive reinforcement configuration, a composite solution could be proposed (fibres + bars). On one hand, the load  $F_c$  ( $F_{w=0.25mm}$  in case of SBFRC) would be reached thanks to the use of fibres. On the other hand, the steel bars would guarantee higher failure strength due to their higher efficiency and strategic position within the section.

**Figure 7 –  $F-v_c$  curves for the pipes with  $D_i = 400$  mm and different reinforcement configurations**

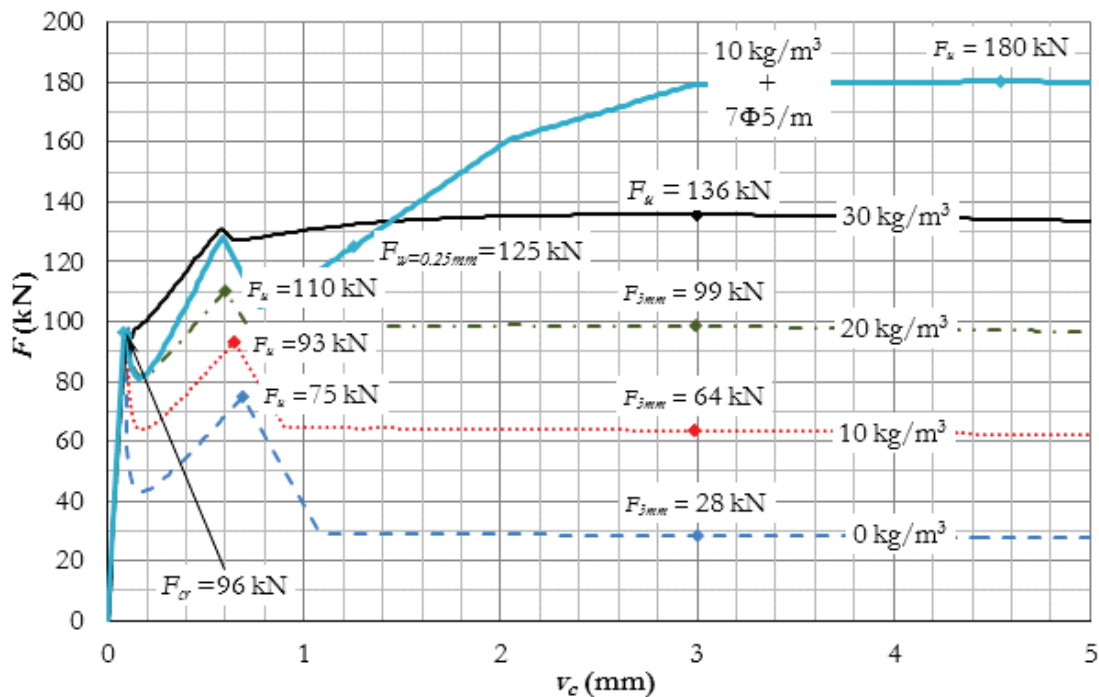


Fig. 7 also shows a simulation considering a reinforcement consisting of 10 kg/m<sup>3</sup> of fibres and 7Φ5/ml of CA60 steel bars. This strategy leads to an  $F_{w=0.25mm} = 125$  kN ( $F_c = 120$  kN) and also to an ultimate failure load  $F_u$  strictly equal to 180 kN. Consequently, class EA4 would be reached, with  $F_u$  being in this case the critical parameter in the design process.

When comparing the curve  $F-v_c$  obtained SFRCP with 30 kg/m<sup>3</sup> of fibres and the one obtained for the SBRCP (10 kg/m<sup>3</sup> + 7Φ5/ml) for values of  $v_c$  up to 1.2 mm (service range), it can be observed that the behavior of the former is better. This highlights the fact that the normative prescription which refers to the load  $F_c$  is much more restrictive for FRCP, if compared with the conventional SBRCP. While FRCP are not allowed any cracking symptoms ( $F_{cr} > F_c$ ), the SBRCP are allowed to reach cracking with a width of up to 0.25 mm ( $F_{w=0.25mm} > F_c$ ). In the opinion of the authors, this criterion restricts the range of application of fibres to this product. Besides, it is not in accordance with the experimental and numerical results, especially when it is known that the inclusion of the suitable type and volume of fibres improves considerably the cracking behavior of the concrete structures.

## 6. Conclusions

This paper introduces the MAP model for the analysis of concrete pipes with mid-low diameters (lower than 1000 mm) and reinforced with traditional steel rebars and/or steel fibres. The bases for this model were already introduced by Pedersen [22], but this paper uses the most recent constitutive equations to simulate the behavior of SFRC. The obtained degree of correlation between experimental and model results can be considered excellent, having obtained numerical results with an average relative error of 7.0% in the safe of safety. To improve this aspect, the constitutive equation of tensioned SFRC could be adjusted taking into account that the fibres are oriented towards a preferential direction within the wall of the pipe. In short, the MAP model can be considered to be a suitable tool for designing the optimal configuration of the reinforcement for this type of pipes. It is intended to be used in precast plants where the required technology to manufacture and test pipes is available. It leads to savings as regards both time and economical resources, since it avoids the extensive test programs required in order to find the optimal amount of reinforcement. This model is especially interesting when a geometrical condition of the pipe, the type of fibres or the strength class is modified, or simply if the factory wishes to make the design tables of the most commercial pipes.

With the aim of illustrating the model capability, an example of optimal design for a pipe with a diameter of 400 mm has been included. The conclusions established were that, according to the model, class EA2 would be obtained with 10 kg/m<sup>3</sup> of fibres; class EA3, with 30 kg/m<sup>3</sup>; and with 10 kg/m<sup>3</sup> + 7Φ5/ml of CA60 steel, class EA4 from the NBR 8890:2007 would be also reached.

Nowadays, several experimental campaigns are being carried out with the purpose of expanding the data bank used to contrast the model and adjust, if necessary, the convenient bases or parameters.

## 7. Acknowledgements

The authors of this document wish to express their appreciation for the financial support received through the Research Project BIA2010-17478: Procesos constructivos mediante hormigones reforzados con fibras.

Likewise, Professor Antonio D. de Figueiredo wishes to thank the support provided by CAPES -Coordenação de Aperfeiçoamento de Pessoal de Nível Superior- for having awarded him the post-doctoral grant that allowed him to participate in this work.

## 8. References

- [01] VIÑOLAS, V., AGUADO, A., JOSA, A. Evaluación de la sostenibilidad en tuberías de saneamiento. II Congreso UPC Sostenible 2015, Barcelona, Spain, 2009.
- [02] HAKTANIR, T., ARI, K., ALTUN, F., KARAHAN, O. A comparative experimental investigation of concrete, reinforced-concrete and steel-concrete pipes under three-edge-bearing test. *Construction and Building Materials*, 2007, vol. 21, n° 8, p. 1702-1708.
- [03] DE LA FUENTE, A., ARMENGOU, J. Aplicaciones estructurales del HRFA: Tubos de saneamiento, paneles de cerramiento y placas de suelo reforzado. *Aplicaciones estructurales del HRFA, Jornada Técnica 2007-JT-02*, 9 de Octubre de 2007, Barcelona: Departamento de Ingeniería de la Construcción, ETS Ingenieros de Caminos, Canales y Puertos, UPC, 2007.
- [04] DE LA FUENTE, A., LARANJEIRA, F., AGUADO, A., MOLINS, C. Structural applications of SFRC. Numerical model for sewer pipes, 2nd National Congress of precast concrete. Centro de Congressos do LNEC, Lisboa, Portugal, 2008.
- [05] FIGUEIREDO, A.D. de. Evaluation of the test method for crushing strength of steel fibre reinforced concrete pipes. 7th International RILEM Symposium on Fibre Reinforced Concrete, Chennai, India, 2008.
- [06] FIGUEIREDO, A.D. de, CHAMA NETO, P.J. Avaliação de desempenho mecânico de tubos. *Revista DAE*, 2008, Vol. 178, p. 34-39.
- [07] LAMBRECHTS, A. Performance classes for steel fibre reinforced concrete: Be critical, 7th International RILEM Symposium on Fibre Reinforced Concrete, Chennai, India, 2008.
- [08] AS'AD, S., SAXER, A. Influence of Fibre Geometry on the Flexural Strength Performance of Steel Fibre Reinforced Concrete (SFRC), *Fibre Concrete 2007*, Prague, Czech Republic, 2007.
- [09] BLANCO, A. Durability of steel fibre reinforced concrete. Minor Thesis, UPC, Barcelona, España, 2008.
- [10] CHIAIA, B., FANTILLI, A.P. VALLINI, P. Evaluation of crack width in FRC structures and application to tunnel linings. *RILEM Materials and Structures*, 2009, Vol. 42, n° 3, p. 339-351.
- [11] BLANCO, A., PUJADAS, P., de la FUENTE, A., AGUADO, A. Comparative analysis of constitutive models of fibre reinforced concrete. *Hormigón y Acero*, 2010, Vol. 61, n° 256, p. 83-100.
- [12] DE LA FUENTE, A., AGUADO, A., MOLINS, C. Integral optimum design of concrete pipes. *Hormigón y Acero*, 2010, Vol. 61, n° 259. [In press].
- [13] FIGUEIREDO, A.D. de, de la FUENTE, A., AGUADO,

- A., MOLINS, C.; VIÑOLAS, B. Análise da viabilidade do uso de fibras metálicas em tubos de concreto. Parte 1: campanha experimental, 52° Congresso Brasileiro do Concreto, IBRACON, Fortaleza, 2010.
- [14] PARROT, J. Sustainability research in sewage pipes, Minor Thesis, UPC, Barcelona, España, 2009.
- [15] HILLERBORG, A., MODÉER, M., Petersson, P.E. Analysis of crack formation and crack growth in concrete by means of fracture mechanics and finite elements. *Cement and Concrete Research*, 1976, Vol. 6, pp. 773-782.
- [16] VANDEWALLE, L. et al. Test and design methods for steel fibre reinforced concrete.  $\sigma$ - $\epsilon$  design method. *RILEM Materials and Structures*, 2003, vol. 36, p. 560-567.
- [17] LARANJEIRA, F., AGUADO, A., MOLINS, C. Equação constitutiva de betão reforçado com fibras, 2° Congresso Nacional de Prefabricação em Betão, Lisboa, Portugal, 2008.
- [18] PEDERSEN, C. Fibre reinforced concrete pipes. *UNICON beton I/S*. December 1992.
- [19] FIGUEIREDO, A.D. de, et al. Steel fibre reinforced concrete pipes. Part 1: technological analysis of the mechanical behavior. *Revista RIEM*, 2011, no prelo.
- [20] ASSOCIAÇÃO BRASILEIRA DE NORMAS TÉCNICAS. Tubo de concreto de seção circular, para águas pluviais e esgotos sanitarios. NBR 8890, ABNT, Rio de Janeiro. 2007.
- [21] DE LA FUENTE, A., AGUADO, A., MOLINS, C. Numerical model for the non linear analysis of precast and sequentially constructed sections. *Hormigón y Acero*, 2008, Vol. 57, n° 247, p. 69-87.
- [22] PEDERSEN, C. Calculation of FRC pipes based on the fictitious crack model. Department of Structural Engineering. Technical University of Denmark, 1995.
- [23] MARÍ, A., BAIRÁN J. Evaluación de los efectos estructurales del deterioro, reparación y refuerzo, mediante análisis no lineal evolutivo. *Hormigón y Acero*, 2009, Vol. 60, n° 254, p. 51-63.
- [24] HEGER, F.J. A theory for the structural behavior of reinforced concrete pipes, PhD Thesis, Department of Civil and Sanitary Engineering, Massachusetts Institute of Technology, MIT, Massachusetts, USA, 1962.
- [25] THORENFELDT, E., TOMASZEWICZ, A., JENSEN J.J. Mechanical properties of high-strength concrete and application in design, Proceedings of the Symposium Utilization of High Strength Concrete, Stavanger, Norway, 1987.
- [26] COLLINS M.P.; MITCHELL, D. Prestressed concrete basics. Canadian Prestressed Institute, Ontario (Canada), 1987.
- [27] BENCARDINO, F.; RIZZUTI, L.; SPADEA, G.; SWAMY, R.N. Stress-strain behavior of steel fibre-reinforced concrete in compression. *ASCE J. of Materials in Civil Engineering* 2008, 20(3):255-63.
- [28] BARROS, J.A.O., FIGUEIRAS, J.A. Flexural behavior of SFRC: Testing and modelling. *ASCE Journal of Materials in Civil Engineering*, 1999, Vol. 11, n° 4, p. 331-339.
- [29] PUJADAS, P. Durability of polypropilene fibre reinforced concrete. Minor Thesis, UPC, Barcelona, España, 2008.
- [30] PEDERSEN, C. The moment-rotation relationship with implementation of stress-crack width relationships. Department of Structural Engineering. Technical University of Denmark, 1995.
- [31] OLESEN, J.F. Fictitious crack propagation in fibre-reinforced concrete beams. *J. of Engineering Mechanics*, 2001, Vol. 127, n° 3, p. 272-280.
- [32] CASANOVA, P., ROSSI, P. Analysis and design of steel fibre reinforced concrete beams. *ACI Structural J.*, 1997, Vol. 94, n° 5, p. 595-602.
- [33] YANG W.Y., WENWU C., CHUNG T.S., MORRIS J. Applied numerical methods using Matlab. John Wiley & Sons Inc., Hoboken, New Jersey, 2005.
- [34] TIMOSHENKO, S. Strength of Materials: Part 1: Elementary Theory and Problems. D. Van Nostrand Inc., New York, N.Y. 1940.
- [35] VANDEWALLE, L. et al., Recommendations of RILEM TC162-TDF: Test and design methods for steel fibre reinforced concrete: Bending test (final recommendation). *Materials and Structures*, 2002, Vol. 35, p. 579-582.
- [36] BARROS, J.A.O., CUNHA, V.M.C.F., RIBEIRO, A.F., ANTUNES, J.A.B. Post-cracking behavior of steel fibre reinforced concrete. *Materials and Structures*, 2005, Vol. 38, p. 47-56.
- [37] COMISIÓN PERMANENTE DEL HORMIGÓN (Ministerio de Fomento). EHE 2008 Instrucción del Hormigón Estructural, 2008.
- [38] DE LA FUENTE, A., AGUADO, A., MOLINS, C. Aplicaciones del HRFA: Tuberías de hormigón. IV Congreso de la asociación científico – técnica del hormigón estructural, Valencia, España, 2008.
- [39] LARANJEIRA, F. Design-oriented constitutive model for steel fibre reinforced concrete. PhD Thesis, UPC, Barcelona, España, 2010.

## 9. Nomenclature

$A$ :	Pipe spigot.
$A_c$ :	Concrete area.
$A_{s,i}$ :	Area of the $i$ -th steel bar.
$B$ :	Pipe socket.
$dA_c$ :	Differential concrete area.
$C_f$ :	Fibre dosage.
$D_i$ :	Internal diameter of the pipe.
$D_o$ :	Outside diameter of the pipe.
$E_{cm}$ :	Average Young modulus of the concrete.
$E_s$ :	Young modulus of the steel.
$F$ :	Applied load on the pipe.
$F_c$ :	Proof load of the pipe.
$F_{cr}$ :	First cracking load of the pipe.
$F_n$ :	Minimum failure load (established) of the pipe.
$F_{max,pos}$ :	Maximum post-failure load (simulated) of the pipe.
$F_{min,pos}$ :	Minimum post-failure load (established) of the pipe.
$F_u$ :	Ultimate failure load of the pipe.
$F_{3mm}$ :	Post-failure load for a 3.0 mm vertical displacement of the key (2 <sup>st</sup> series of the tested pipes).

$f_{ck}$ :	Characteristic compressive concrete strength.	$x_n$ :	Neutral axis depth.
$f_{cm}$ :	Average compressive concrete strength.	$y$ :	Height of the analyzed element.
$f_{ctm,fl}$ :	Average flexural tensile concrete strength.	$y_c$ :	Height of the analyzed concrete layer.
$f_{Ri}$ :	Residual flexural concrete strength.	$y_G$ :	Height of the gravity center of the section.
$f_{s,max}$ :	Maximum steel strength.	$y_{s,i}$ :	Height of the analyzed $i$ -th steel bar.
$f_y$ :	Yielding strength of the steel.	$\beta$ :	Angle between the supports and the centre of the pipe.
$h$ :	Thickness of the concrete wall.	$\varepsilon$ :	Strain.
$I$ :	Moment of inertia around the horizontal axis ( $I = h^3/12$ ).	$\varepsilon_c$ :	Concrete strain.
$k_h$ :	Size factor.	$\varepsilon_s$ :	Tensile strain of the SFRC.
$l$ :	Length of the pipe.	$\varepsilon_c^m$ :	Mechanical concrete strain.
$l_{bc}$ :	Length of the hinge.	$\varepsilon_c^{nm}$ :	Non-mechanical concrete strain.
$M$ :	Applied bending moment.	$\varepsilon_s$ :	Steel strain.
$M_c$ :	Bending moment at ridge.	$\varepsilon_{c,sup}$ :	Strain of the concrete section top layer.
$M_s$ :	Bending moment at springline.	$\varepsilon_{c,inf}$ :	Strain of the concrete section bottom layer.
$M_\theta$ :	Bending moment at the angular coordinate $\theta$ .	$\varepsilon_{s,i}$ :	Strain of the $i$ -th steel bar.
$N$ :	Applied normal force.	$\varepsilon_y$ :	Yielding steel strain.
$N_\theta$ :	Normal force at the angular coordinate $\theta$ .	$\theta$ :	Angular coordinate.
$n_s$ :	Number of steel bars.	$\xi$ :	Relative error of the numerical value.
$R_m$ :	Average radius of the pipe.	$\sigma_c$ :	Concrete stress.
$s_n$ :	Height of the crack.	$\sigma_f$ :	Steel fibre concrete tension stress.
$t$ :	Instant of calculus.	$\sigma_s$ :	Steel stress.
$t_o$ :	Age of loading.	$\sigma_{s,i}$ :	$i$ -th steel bar stress.
$u_s$ :	Horizontal displacement of the springline.	$\sigma_u$ :	Ultimate concrete compressive stress.
$u_s^e$ :	Elastic horizontal displacement of the springline.	$\varphi$ :	Angle between the crack faces.
$u_s^p$ :	Plastic horizontal displacement of the springline.	$\varphi_c$ :	Rotation of the ridge.
$v_c$ :	Vertical displacement of the ridge.	$\varphi_c^{crk}$ :	Cracking rotation of the ridge.
$v_c^e$ :	Elastic vertical displacement of the ridge.	$\varphi_s$ :	Rotation of the springline.
$v_c^p$ :	Plastic vertical displacement of the ridge.	$\varphi_s^{crk}$ :	Cracking rotation of the springline.
$v_{c,max}$ :	Maximum vertical displacement of the ridge.	$\chi$ :	Sectional curvature.
$w$ :	Crack width.	$\chi_c$ :	Curvature of the section of the ridge.